LC3 and NLRC5 Interaction Inhibits NLRC5-Mediated MHC Class I Antigen Presentation Pathway in Endometrial Cancer

Lei Zhan
First Affiliated Hospital of Anhui Medical University
Junhui Zhang
First Affiliated Hospital of Anhui Medical University
Jing Zhang
Second Affiliated Hospital of Anhui Medical University
Xiaojing Liu
Second Affiliated Hospital of Anhui Medical University
Suding Zhu
Second Affiliated Hospital of Anhui Medical University
Yuchuan Shi
Second Affiliated Hospital of Anhui Medical University
Yu He
Second Affiliated Hospital of Anhui Medical University
Wenyan Wang
Second Affiliated Hospital of Anhui Medical University
Yijun Fan
Second Affiliated Hospital of Anhui Medical University
Zhenhai Tang
Anhui Medical University
Guo Chen
Maternal and Child Health Hospital of Anhui Medical University
Bing Wei (m1351565@163.com)
The Second Affiliated Hospital of Anhui Medical University https://orcid.org/0000-0003-0337-5775
Yunxia Cao
First Affiliated Hospital of Anhui Medical University

Research

Keywords: LC3, NLRC5, MHC-I, Antigen presentation, Immune evasion, Immunotherapy

Posted Date: November 10th, 2021

DOI: https://doi.org/10.21203/rs.3.rs-1018081/v1

Version of Record: A version of this preprint was published at Cancer Letters on December 1st, 2021. See the published version at https://doi.org/10.1016/j.canlet.2021.12.031.

Abstract

Background: The major histocompatibility complex class I (MHC- I) transactivator, nucleotide binding oligomerization domain-like receptor family caspase recruitment domain containing 5 (NLRC5), serves as a target for immune evasion in many cancers, including endometrial cancer (EC). An inhibition of autophagy can contribute to immunotherapy by assisting the MHC-I-mediated antigen presentation in cancer. However, the underlying mechanism for autophagy-regulated MHC-I in EC remains unclear. Our study aimed to investigate the effect of autophagy on NLRC5 and MHC-I-mediated antigen presentation, and to identify the potential mechanisms underlying this process in EC.

Methods: We examined the levels of autophagy and MHC-I genes by performing transmission electron microscopy (TEM), RNA-seq sequencing, western blotting, and qRT-PCR. The *t*-test, F-test, Kaplan-Meier analysis, and Pearson's correlation analysis were used for statistical evaluations of tissue microarrays. Immunofluorescence staining, co-immunoprecipitation (CO-IP), and glutathione S-transferase (GST) pull-down assay were performed. HEC-1A, AN3CA, and Ishikawa EC cells were transfected designed, and the role of LC3 and NLRC5 in MHC-I-mediated antigen presentation in EC was further evaluated in a xenotransplantation model of HEC-1A cell line.

Results: Autophagy was upregulated in EC endometrium as compared to that in normal endometrium. MHC I and NLRC5 expressions were lower in EC endometrium than in normal endometrium. Autophagy played a negative role in the MHC-I genes expression *in vitro*. Furthermore, a negative correlation was found between LC3 and NLRC5 levels, and LC3 interacted with NLRC5 to inhibit NLRC5-mediated MHC-I antigen presentation pathway *in vitro* and *in vivo*.

Conclusion: An upregulation of LC3 in EC patients may contribute to tumor immune escape by restricting the NLRC5-mediated MHC-I antigen presentation pathway, suggesting that inhibiting LC3 and promoting NLRC5 may be a promising immunotherapy strategy in the management of EC.

Background

Uterine cancer, one of the most common gynecological cancer, is the 5th leading cause of cancer death in the United States [1]. The latest reports indicate that its incidence in young women is rising, and in 2020 in United States, approximately 79,420 women have been diagnosed with uterine cancer and 16,880 people have died because of uterine cancer [2]. The most common uterine cancer is endometrial cancer (EC). Although EC patients demonstrate a five-year survival rate of 81% (2009-2015), the survival rate is remarkably reduced in patients with obesity and patients with metastasis or recurrence [2, 3]. Obesity, hypertension, diabetes, and Lynch syndrome are the major risk factors that are associated with the pathogenesis of EC [4]. Surgical resection and chemoradiotherapy are the main treatment options for EC; however, they are ineffective in the advanced stage EC [5]. Importantly, researchers have discovered a novel treatment, known as tumor immunotherapy, which trains the body's immune system to kill the tumor cells but not the healthy cells [6]. The success of immunomodulation on the basis of immune checkpoint inhibitors and chimeric antigen receptor-T cell has generated an increased interest regarding its potential to treat EC [7]. In recent years, immunotherapy for EC has been widely investigated, and pre-clinical studies and clinical trials have revealed

its promising potential [8, 9]. However, some obstacles occur during tumor immunotherapy, and one of the most difficult problems is the immune escape of tumor cells [10].

Several different mechanisms have been reported for the escape of tumor cells from immune surveillance [11]. Among them, the loss of major histocompatibility complex class I (MHC-I) is a crucial immune evasion strategy in tumors [12]. Recently, it has been reported that nucleotide binding oligomerization domain (NOD)-like receptor family caspase recruitment domain containing 5 (NLRC5), known as MHC-I transactivator, is a novel target for the earliest immune evasion in tumors [13]. Loss of NLRC5 in cancer is closely related to downregulation of MHC-I genes and impaired cytotoxic T cell activities. Tumor cells suppress MHC-I genes *via* NLRC5 methylation, but not *via* the direct methylation of MHC-I genes, suggesting an essential relevance of NLRC5 with tumor immune evasion [13]. Recruitment of NLRC5 contributes to tumor antigens presentation to $CD8^+$ T cells, which further increases antitumor immunity [14]. Therefore, NLRC5-mediated MHC-I antigen presentation pathway is a potential immunotherapeutic target for cancer.

Autophagy involves the cellular pathways that deliver intra- and extracellular products for lysosomal degradation, which benefit innate and adaptive immunity, indicating a promising role of autophagy in immunotherapy [15]. Evidence suggests that autophagy influences cellular immune responses; however, the role of autophagy in immune responses remains controversial. It has been reported that defective autophagy in triple-negative breast cancer cells inhibits T cell-mediated tumor killing *in vitro* and *in vivo* [16]. However, in viral infection models, a loss of autophagy upregulates the levels of MHC-I genes in dendritic cells, which further leads to an enhanced $CD8^+$ T cell response [17]. Recently, it has been suggested that autophagy-mediated MHC-I degradation facilitates immune evasion in pancreatic ductal adenocarcinoma and autophagy inhibition reduces tumor growth and increases tumor infiltration by $CD8^+$ T cells [18]. However, the molecular mechanism underlying autophagy in MHC-I-mediated tumor antigen presentation has not yet been elucidated. Our previous study on endometriosis revealed a negative correlation between autophagy related proteins and NLRC5, indicating a potential role of autophagy in NLRC5 [19]. In our present study in EC patients, we investigated the correlation between autophagy and NLRC5. We also explored the role and mechanism by which autophagy regulating NLRC5-mediated MHC-I antigen presentation pathway in EC cells and a xenotransplantation model of HEC-1A cell line.

Materials And Methods

Transmission electron microscopy (TEM)

The study was approved by the Institutional Review Board of Anhui Medical University (No: 20180023). A written informed consent was obtained from all patients prior to sample collection and storage. EC tissues were obtained from the EC patients with total hysterectomy with bilateral salpingo-oophorectomy. Normal endometrium were obtained from biopsies taken for the investigation of reproductive problems. All patients did not undergo chemotherapy, radiotherapy, biotherapy, or any other operation prior to surgery. Endometrial tissues and EC cells were fixed using 2% glutaraldehyde, rinsed with 100 mM cacodylate buffer (pH 7.4), fixed with 1% OsO_4 in cacodylate buffer, dehydrated with gradient ethanol (50%, 70%, 80%, 90%, 95%, 100%) at 25 °C, and embedded in Eponate. Ultra-thin sections exposure to double staining with uranyl

acetate and 1% lead citrate, and images were captured using a transmission electron microscope (HT7700, Hitachi High Technologies, Japan).

Briefly, the total RNA was isolated from EC and normal tissues using TRIzol reagent (Takara Bio, Japan). On the denaturing agarose gel, electrophoresis were used to validate RNA integrity and DNA contamination. Using pretreated RNAs with TruSeq Stranded Total RNA Library Prep Kit (Illumina, San Diego, CA, USA), RNA-seq libraries were constructed. The libraries were denatured as single-stranded DNA, bound to the surface of Illumina flow cells, amplified in situ as clusters and finally sequenced for 150 cycles on Illumina HiSeq™ 4000 Sequencer (Illumina, San Diego, CA, USA).

Western blotting

Cells were lysed using the protein extraction solution (Beyotime). Protein concentration was calculated using the BCA assay kit (Sino Biotech, China). Cell lysates were obtained using centrifugation speeds of 12000rpm at 4 °C for 30 min, and they were transferred onto polyvinylidene difluoride membranes (Millipore Corp, Billerica, MA, USA). After blocking the membranes, nitrocellulose blots were incubated for 6 h with primary antibodies diluted in a primary antibody dilution buffer (Beyotime). The primary antibodies recognizing LC3 (ab192890, Abcam), Beclin1 (ab207612, Abcam), P62 (18420-1-AP, Proteintech), NLRC5 (DF13672, Affinity), human leukocyte antigen A (HLA-A, ab52922, Abcam), low molecular mass polypeptides 2 (LMP2, ab184172, Abcam), transporter associated with antigen processing 1(TAP1, ab83817, Abcam), beta-2-microglobulin (β2-M, ab75853, Abcam), and β-actin (GB12001, Servicebio) were used at 1:1000, 1:1000, 1:1000, 1:1000, 1:1000, 1:1000, 1:1000, 1:1000, 1:1000, and 1:5000 dilutions, respectively. The membranes were incubated in Tris-buffered saline with 0.1% Tween 20 (TBST, Boster Bio, China) containing 5% skim milk at 37 °C for 4 h, and subsequently, they were incubated with specific primary antibodies at 4 °C overnight. Next, the membranes were washed thrice with TBST, and they were incubated with -conjugated secondary antibodies (Thermo Fisher Scientific, 1:10000) at 37 °C for 1 h. After washing thrice with TBST, the proteins were visualized using an ECL chemiluminescent kit (ECL-plus, Thermo Fisher Scientific). The protein levels of LC3-II, which represent the protein levels of LC3, were measured. All experiments were performed in triplicate, and they were repeated at least thrice.

RNA extraction and qRT-PCR

Total RNA was collected from cultured cells using the TRIzol reagent (Takara Bio, Japan), following the manufacturer's instructions. First-strand cDNA was synthesized using a Thermoscript RT-PCR synthesis kit (Fermentas, USA). qRT-PCR analyses for the mRNAs of LC3, Beclin1, P62, NLRC5, HLA-A, LMP2, TAP1, β2-M, and β-actin were performed using Thermoscript qRT-PCR kits (Fermentas) in an ABI Prizm step-one plus real time PCR System (Applied Biosystems, USA). The β-actin mRNA level was used as an internal control. Relative expression levels were calculated based on the standard $2^{-\Delta\Delta Ct}$ method. All experiments were performed in triplicate, and they were repeated at least thrice. qRT-PCR primers are listed in Table 1.

Cell culture

The human EC cell lines HEC-1A, AN3CA, and Ishikawa cells were obtained from American Type Culture Collection, and they were cultured in RPMI-1640 medium (Invitrogen, USA) containing 10% fetal bovine serum (FBS; HyClone, Logan, UT, USA) under 5% CO_2 at 37 °C.The LC3 plasmid, LC3 plasmid (GFP) + NLRC5 plasmid (RFP, LC3+NLRC5), shRNA-LC3 (GFP), shRNA-NLRC5 (RFP) were constructed, and the RNA sequences of LC3 plasmid, shRNA-LC3, NLRC5 plasmid, and shRNA-NLRC5 are presented in Table 2. LC3 plasmid, shRNA-LC3, NLRC5 plasmid, and shRNA-NLRC5stably expressing HEC-1A, AN3CA, Ishikawa cells were cultured in RPMI-1640 containing 10% FBS and 2 μg/mL (Sigma, USA) under 5% CO_2 at 37 °C.Western blotting and quantitative reverse transcription PCR (qRT-PCR)were performed to validate the stable expression of HEC-1A, AN3CA, and Ishikawa cellsin LC3 plasmid, shRNA-LC3, NLRC5 plasmid, and shRNA-NLRC5.

Treatment with the autophagy agonist, rapamycin, or autophagy inhibitor, chloroquine (CQ)

Rapamycin (100 nM, Sigma) and CQ (20 mM, Sigma) were dissolved in dimethyl sulfoxide (Sigma) according to the methods described in previous studies [20, 21]. HEC-1A, AN3CA, and Ishikawa cells were seeded overnight in culture dishes, and they were treated with rapamycin or CQ for 48 h.

Immunofluorescence staining

HEC-1A, AN3CA, Ishikawa, and their shRNA-NLRC5 cells were fixed in 4% paraformaldehyde (Sigma) for 30 min, washed with phosphate buffered saline (PBS), and then permeabilized with 0.1% Triton X-100 (Thermo Fisher Scientific) for 20 min. Subsequently, primary antibodies, anti-NLRC5 (DF13672, Affinity) and anti-LC3 (GB11124, Servicebio) were added, and they were incubated at 37 °C for 45 min. After incubation, the antibody solution was discarded, and each section was washed thrice with immunohistochemical washing solution (Beyotime, Shanghai, China) at room temperature for 5 min. Next, secondary antibodies were added, and the tissues were incubated at 37 °C for 45 min. After incubation, the antibody solution was discarded, and each section was washed thrice with immunohistochemical washing solution at room temperature for 5 min. Finally, the immunofluorescence blocking solution (Sigma) was added, sections were mounted, and images were captured using a confocal laser-scanning microscope (Nikon, Eclipse Ti-U, Japan). The double immunofluorescence staining of NLRC5 (DF13672, Affinity) and MHC I (ab281903, Abcam, Cambridge, MA, USA) in NLRC5 HEC-1A cell was operated as above described.

Co-immunoprecipitation (CO-IP)

The interactions between LC3 and NLRC5 in HEC-1A, AN3CA, and Ishikawa cells were investigated using CO-IP. Briefly, anti-LC3-labeled beads were co-incubated with HEC-1A, AN3CA, and Ishikawa cells. After 6 h of incubation, the beads were washed twice with TBST, and subsequently, they were eluted with 2XNRSB buffer (Thermo Fisher Scientific) at 95 °C. The eluates were analyzed using western blotting with antibodies against LC3 () and NLRC5 (sc-515668, Santa Cruz, USA).

Glutathione S-transferase (GST) pull-down assay

The interactions between LC3 and NLRC5 were further determined using a GST pull-down assay. The plasmids for GS-NLRC5 and His-LC3 were transfected into *Escherichia coli.* GST, GST fusion proteins, and NLRC5 were constructed and purified with glutathione Sepharose 4B beads (Sigma). The His-LC3 fusion protein was purified, and it was collected using Ni-NTA beads (Sigma). His-LC3 protein was rotated with GST and GST-NLRC5 at 4 °C for 4 h, and subsequently, the mixture was added to Ni-NTA beads at 4 °C for an additional 4 h. After centrifugation speeds of 3000rpm at 4 °C for 2 min and three washes, the beads were eluted with 30 μL of 1×SDS-PAGE loading buffer (Thermo Fisher Scientific), and subsequently, they were boiled for 10 min and analyzed using western blotting.

tissue microarray

Tissue microarrays consisting EC endometrial tissues and thirty-six normal endometrial tissues were examined in the study. Clinical information of EC patients include age, body mass index (BMI), menopausal status, histological subtype, tumor stage, tumor grade, myometrial invasion, and lymph node metastasis. Tumor stage was determined according to the 2009 International Federation of Gynecology and Obstetrics (FIGO) criteria. Histological subtype and tumor grade were assessed according to the World Health Organization guidelines. Clinical information of thirty-six normal endometrial include age and BMI.

Immunohistochemistry

Immunohistochemistry assay was performed as previously described to measure the expression levels of LC3 and NLRC5. Briefly, tissue microarray sections were dewaxed and dehydrated in xylene and alcohol respectively, and antigen recovery was accomplished by microwaving in citric saline for 15 min. Subsequently, the sections were deparaffinized and deal with 0.3% hydrogen peroxide for 15 min to suppress endogenous peroxidase activity. Furthermore, the sections were blocked with 2% bovine serum albumin, then incubation with primary rabbit monoclonal antibodies against LC3 (GB11124, Servicebio, diluted 1:500) and NLRC5 (DF13672, Affinity, diluted 1:100) at 4 °C for 16 h. After rinsing, microarray sections were incubated with a biotinylated secondary antibody (G1210-2-A, Servicebio) at 20-25°C temperature for 60 minutes. LC3 and NLRC5 expression levels were visualized using 3, 3$^{¢}$-diaminobenzidine tetrahydrochloride staining. Slides were counterstained with hematoxylin before dehydration and mounting. Quantitative analyses were conducted for five random fields at ×200 magnification for each endometrial tissue slice. All sections were observed under the Axioscope A1 microscope (Carl Zeiss, Germany) and photographed. The background light of each photo was consistent. Dark brown staining indicated a positive reaction. The intensity of dark brown staining was analyzed using Image-Pro plus 6.0 (Media Cybernetics, Inc.).

Flow cytometry

To analyze the $CD8^+$ T cell among $CD45^+$ cells from the of mice, $CD8^+$ T cells were collected and concentrated, and they were incubated with 5 μL of specific fluorescent CD8 antibody (100705, Biolegend, USA) and specific fluorescent CD45 antibody (368507, Biolegend) for 20 min. Saline (500 μL) was added separately into the cell solution, which was followed by centrifugation at 5000 rpm for 5 min. The supernatant was removed, and the collected cells at the bottom were dispersed into 300 μL of saline. Finally, the effective separation rate was analyzed by counting 1.2×10^4 cells per sample using an LSR II flow cytometer (BD Biosciences, CA, USA) and Cell Quest software (BD Biosciences).

$CD8^+$ T cell proliferation assay

CD8 T^+ cell was purified from peripheral blood mononuclear cells (PBMCs) of healthy female volunteers. Cell purity was checked. $CD8^+$ T cellwas labeled with 1μM CFSE (S8269, selleck, USA) and stimulated with CD3/CD28 antibody and co-cultured with vector transfected, LC3plasmid, and LC3 + NLRC5 HEC-1A cells, in 96-well plates at a ratio of 5: 1 for 3 days. $CD8^+$ T cell was collected, and the dilution of intracellular CFSE caused by proliferation was calculated using flow cytometry.

Enzyme-linked immune sorbent assay (ELISA)

The expression levels of $CD8^+$ T cell secreted interferon gamma (IFN-γ), , and interleukin-2 (IL-2) from the of mice according to manufacturer's instructions. Samples were run in duplicates. Inter-assay coefficients of variation were calculated using the results obtained in 10 different assays performed at different time points using different plates. Intra-assay coefficients of variation were calculated for 10 replicates of the sample in the same plate.

In vivo xenograft experiments

six-week-old female BALB/C mice were purchased from Hangzhou Ziyuan Laboratory Animal Science and Technology Co. Ltd, and they were reared in an SPF environment. Following this, 5×10^6 HEC-1A cells transfected with LC3 (n=5), LC3+NLRC5 (n=5), shRNA-LC3 (n=5), or vector transfected (n=5) and suspended in RPMI-1640 medium (Invitrogen, USA) were left armpit subcutaneously injected. The tumor volume was measured twice a week until the tumor could be visually observed. After 4 weeks, the mice were euthanized, and the implanted tumors were removed, measured, and photographed. The tumors were weighed, and the volumes were calculated using the following formula: tumor volume (mm^3)=(ab^2)/2 [a: the longest axis (mm), b: the shortest axis (mm)]. $CD8^+$ T cell among $CD45^+$ cells from the of mice was detected by flow cytometry. The expression levels of $CD8^+$ T cell secreted IFN-γ, , and IL-2 from the of mice were validated using an ELISA kit (R&D Systems, USA), according to manufacturer's instructions. Immunohistochemistry was performed todetect the $CD8^+$ level from the tumor.All animal feeding and *in vivo* experimental procedures were conducted in accordance with the Regulations on Laboratory Animal Management of the Animal Experimental Department of Anhui Medical University, and the animal experiment was approved by the Ethics

Review Committee of the department of Laboratory Animal Science of Anhui Medical University (No: LLSC201800855).

Statistical analysis

All data were analyzed using the SPSS 23.0 software (SPSS Inc., Chicago, USA). Data are expressed as mean ± SEM. Statistical analyses were performed using analysis of variance. Significant differences and variance between groups were identified using using Student *t*-test and F-test respectively. Correlation analysis was performed using Pearson's correlation. The median LC3 and NLRC5 expression was used as a cut-off value for grouping. The survival curves were measured by the Kaplan-Meier method. $P<0.05$ was considered statistically significant.

Results

Autophagy is upregulated and MHC-I genes are downregulated in EC patients

We first detected the levels of autophagy and MHC-I genes in 10 EC endometrium and 10 normal endometrium. The number of autophagosomes was upregulated in endometrium of EC patients as compared to those in normal endometrium (Fig. 1A). The protein and mRNA levels of autophagy proteins LC3 II and Beclin1 were upregulated in endometrium of EC patients as compared to those in normal endometrium (Fig. 1B). RNA-seq sequencing showed MHC-I genes were downregulated in endometrium of EC patients as compared to those in normal endometrium, including HLA-A/B/C, LMP2/7, TAP1, β-2M (Fig. 1C). We further confirmed the levels of HLA-A, LMP2, TAP1, β-2M were decreased in endometrium of EC patients as compared to those in normal endometrium by western blotting and qRT-PCR (Fig. 1D).

Autophagy Inhibits Mhc-i Genes Expression In Ec Cells

To further investigate the role of autophagy in MHC-I genes in EC, we detected HLA-A, LMP2, TAP1, and β-2M expressions at the surface of EC cells by using the autophagy agonist rapamycin, and autophagy inhibitor CQ to promote and restrict autophagy, respectively, in HEC-1A, AN3CA, and Ishikawa cells. We first observed that 100nM rapamycin could activate autophagy effective by promoting LC3 and inhibiting P62 expressions (Fig. 2A), and increasing the number of autophagosomes (Fig. 2B). Then we found rapamycin could inhibit the expressions of HLA-A, LMP2, TAP1, and β2-M in HEC-1A, AN3CA, and Ishikawa cells (Fig. 2C-E).

We also use CQ to inhibit autophagy. We observed that 20 mM CQ could inhibit autophagy effective by promoting LC3 and P62 expressions (Fig. 3A), and increasing the number of autophagosomes and down-regulating the number of autolysosomes (Fig. 3B). Furthermore, CQ could promote the expressions of HLA-A, LMP2, TAP1, and β2-M in HEC-1A, AN3CA, and Ishikawa cells (Fig. 3C-E). These findings suggest that autophagy can inhibit MHC-I genes expression at the surface of EC cells. However, the underlying mechanism of the negative role of autophagy in MHC-I genes expression is still unclear.

Lc3 Interacts With Nlrc5

As NLRC5 is known as an MHC-I transactivator, we examined whether NLRC5 is involved in the negative role of autophagy in MHC-I genes expression. We first found LC3 and NLRC5 were co-localized in the cytoplasm of HEC-1A, AN3CA, and Ishikawa cells by immunofluorescence staining, but no co-localization was found when NLRC5 was knockdown by shRNA-NLRC5 in HEC-1A, AN3CA, and Ishikawa cells (Fig. 4A). Furthermore, the CO-IP assay revealed an interaction between LC3 and NLRC5 in HEC-1A, AN3CA, and Ishikawa cells (Fig. 4B). Additionally, the GST pull-down assay revealed an interaction between LC3 and NLRC5 (Fig. 4C). We also established an endometrial tissue microarray to detect the correlation between LC3 and NLRC5 (Fig. 4D). Demographic characteristics are summarized in Table 3. Immunohistochemistry analysis of tissue microarrays revealed that the LC3 was upregulated in EC tissues as compared to that in normal endometrial tissues (51.42±22.95 *vs* 26.89±11.33, t=6.980, *P*<0.001). NLRC5 expression in the endometrium of EC patients was significantly lower than in the normal endometrium (28.71±17.74 *vs* 51.59±23.79, t=4.997, P<0.001). Pearson's correlation was performed to analyze the correlation between LC3 and NLRC5 expression. The correlation analysis revealed a significant negative correlation between NLRC5 and LC3 (r=-0.233, *P*=0.022). Moreover, we found high expression levels of LC3 (t=3.866, *P*=0.019) and low level of NLRC5 (t=2.978, *P*=0.027) were correlated with positive lymph node metastasis in EC patients. LC3 level was correlated with the FIGO stage (2009) (F=2.960, *P*=0.047) and histological grade (F=3.136, *P*=0.023) in EC patients. However, Kaplan-Meier analysis showed that the expressions of LC3 and NLRC5 were not associated with cumulative survival in EC patients (Fig. 4E).

LC3 negatively regulates NLRC5 and MHC-I genes expressions in EC cells

The above-mentioned results suggest that LC3 can interact with NLRC5. Therefore, we investigated whether LC3 could regulate NLRC5 and the MHC-I genes expressions. LC3 plasmid and shRNA-LC3 HEC-1A, AN3CA, and Ishikawa cells were constructed (Fig. 5A). We found that LC3 plasmid HEC-1A, AN3CA, and Ishikawa cells demonstrated decreased protein level of NLRC5 and decreased protein and mRNA levels of MHC-I genes as compared to those in vector HEC-1A, AN3CA, and Ishikawa cells (Fig. 5B-D).

ShRNA-LC3 HEC-1A, AN3CA, and Ishikawa cells were also constructed (Fig. 6A). We further found that shRNA-LC3 HEC-1A, AN3CA, and Ishikawa cells demonstrated elevated the protein level of NLRC5, and the protein and mRNA levels of MHC-I genes as compared to those in shNC HEC-1A, AN3CA, and Ishikawa cells (Fig. 6B-D). These results suggested that LC3 could negatively regulate NLRC5 and MHC-I genes expressions in EC cells.

LC3 inhibits MHC-I antigen presentation pathway by downregulating NLRC5 in vitro

We further investigated whether LC3 could interact with NLRC5 to inhibit the MHC-I antigen presentation pathway. NLRC5 plasmid HEC-1A cell was constructed (Fig. 7A). Furthermore, NLRC5 plasmid promoted NLRC5 moved to the nucleus of HEC-1A cell (Fig. 7B) and co-localized with MHC-I (Fig. 7C). Overexpression of NLRC5 contributed to the expressions of HLA-A, LMP2, TAP1, and β2-M (Fig. 7D). We used the co-cultured system to validate the role of NLRC5 in MHC-I antigen presentation pathway. Vector and NLRC5 plasmid HEC-1A cells were co-cultured with $CD8^+$ T cell. $CD8^+$ T cell purity was showed in Fig. 7E. We found overexpression

of NLRC5 led to $CD8^+$ T cell proliferation in HEC-1A and $CD8^+$ T cell co-cultured system (Fig. 7F). In addition, LC3+NLRC5 HEC-1A cell demonstrated a restriction in the negative role of LC3 in HLA-A, LMP2, TAP1, and β2-M expressions as compared to that in LC3 plasmid HEC-1A cell (Fig. 7G). We also used the co-cultured system to validate the role and mechanism of LC3 in MHC-I antigen presentation pathway. Vector, LC3 plasmid, and LC3+NLRC5 HEC-1A cells were co-cultured with $CD8^+$ T cell. We found that LC3 plasmid HEC-1A cell demonstrated decreased $CD8^+$ T cell proliferation as compared to those in vector HEC-1A cell. LC3+NLRC5 HEC-1A cell demonstrated a restriction in the negative role of LC3 in $CD8^+$ T cell proliferation as compared to that in LC3 plasmid HEC-1A cell (Fig. 7H). These results suggest that LC3 inhibits MHC-I antigen presentation pathway by downregulating NLRC5.

LC3 inhibits the MHC-I antigen presentation pathway by downregulating NLRC5 expression in vivo

The mice were sacrificed after 5 weeks, and a tumor arising from LC3 plasmid HEC-1A cells showed a more rapid growth than the one from HEC-1A cells, tumor arising from NLRC5 plasmid HEC-1A cell showed a slower growth than that from HEC-1A cells, and tumor arising from LC3+NLRC5 HEC-1A cells showed a slower growth than that from LC3 plasmid HEC-1A cells. Similarly, an assessment of tumor volume and weight in each group of mice revealed that overexpression of LC3 promoted tumor volume and weight, and upregulation of NLRC5 expression restricted the tumor growth by LC3 *in vivo*, overexpression of NLRC5 inhibited tumor volume and weight (Fig. 8A). Consistent with these findings, in mice tumor tissues, the expression levels of NLRC5, HLA-A, LMP2, TAP1, and β2-M in the tumor arising from LC3 plasmid HEC-1A cells were lower than those in the tumor arising from HEC-1A cells. The expression levels of NLRC5, HLA-A, LMP2, TAP1, and β2-M in the tumor arising from NLRC5 plasmid HEC-1A cells were higher than those in the tumor arising from HEC-1A cells, and the expression levels of NLRC5, HLA-A, LMP2, TAP1, and β2-M in the tumor arising from LC3+NLRC5 HEC-1A cell were higher than those in the tumor arising from LC3 plasmid HEC-1A cell (Fig. 8B). The expression of tumor infiltrating $CD8^+$ T cell in mice tumor also consist with the above findings (Fig. 8C). Furthermore, the frequency of $CD8^+$ T cell in $CD45^+$ cell (Fig. 8D) and the production of cytokines, IFN-γ, TNF-α, and IL-2 (Fig. 8E) were lower in the blood of mice with tumors arising from LC3 plasmid HEC-1 cells than in the blood of mic with tumors arising from HEC-1A cells. The frequency of $CD8^+$ T cell in $CD45^+$ cell and the production of cytokines, IFN-γ, TNF-α, and IL-2 were upregulated in the blood of mice with tumors arising from NLRC5 plasmid HEC-1A cells than the blood of mice with tumor arising from HEC-1A cells. The frequency of $CD8^+$ T cell in $CD45^+$ cell and production of cytokines, IFN-γ, TNF-α, and IL-2 were higher in the blood of mice with tumors arising from LC3+NLRC5 HEC-1A cells than in the blood of mice with tumor arising from LC3 plasmid HEC-1A cell. These results suggest that LC3 inhibits MHC-I genes and $CD8^+$ T cell frequency by downregulating NLRC5 expression *in vivo*. Therefore, inhibiting LC3 and overexpression of NLRC5 expression may be promising immunotherapeutic approaches for EC patients by promoting the MHC-I antigen presentation pathway (Fig. 8F).

Discussion

In our present study, we found that autophagy level was upregulated in EC endometrium compared to that in normal endometrium. The level of NLRC5 was lower in EC endometrium than in normal endometrium. Furthermore, a negative correlation existed between LC3 and NLRC5. Autophagy inhibited MHC-I genes

expression *in vitro*. Mechanistic investigations found that LC3 interacted with NLRC5 to inhibit NLRC5-mediated MHC-I antigen presentation pathway *in vitro* and *in vivo*. Our findings highlight a potential immunotherapy approach in EC patients by inhibiting LC3 and promoting NLRC5.

EC is classified into type I, which represents the most common EC and at least 90% of tumors express estrogen receptor moderately or strongly, and type II, which is estrogen-independent and mostly represents serous carcinoma, according to clinicopathological characteristics [1, 22]. However, the histological classification of EC has limitations due to poor reproducibility, and overlapping morphological and immunohistochemical features have been recognized [23]. Now, the Proactive Molecular Risk Classifier for Endometrial Cancer utilizes immunohistochemistry to reclassify EC into polymerase ε-mutated, mismatch-repair-deficient, p53 abnormalities, and p53 wildtype, which is more suitable for clinical application and better predicts the clinical responses to immunotherapy [24]. Immunotherapy is an emerging clinical approach that has gained attention over the past decade, resulting in new treatment options for lung cancer and melanoma. These achievements are a good reason for humans to explore immunotherapy for EC [25]. Indeed, clinical trials have explored several immunotherapeutic strategies for EC, such as vaccines [26] and immune checkpoint inhibitors [9]. Unfortunately, only a handful of patients show a good therapeutic response because of immune escape in EC. The mechanisms of immune evasion in EC include inhibiting T lymphocytes and natural killer cells activity [27, 28], gene mutations [29], and loss of MHC-I genes [30].

Generally, the tumor antigen presentation to $CD8^+$ T cells by MHC-I genes is essential for immune responses against cancers [31]. NLRC5 is well studied as a transcriptional regulator of MHC-I genes in immune cells, and it shuttles between the cytoplasm and nucleus to play a leading role in the modulation of MHC-Idependent immune responses [32]. Previous studies have suggested that NLRC5 is a target for immune evasion in cancer [13]. Recently, it has been suggested that IFN-γ stimulation can promote NLRC5 expression with an upregulation of MHC-I genes expression in MHC-I-deficient breast cancer cells [33]. By analyzing 7,747 patients with solid cancer and 21 solid cancer types, Yoshihama and co-workers reported that NLRC5 was essential for MHC I-dependent $CD8^+$ T cell-mediated tumor immunity [13]. Furthermore, upregulation of NLRC5 expression is correlated with an increased survival in multiple cancer types [13]. In our study, we found that the expression of NLRC5 and MHC-I genes in the endometrium of EC patients was significantly lower than in the normal endometrium, suggesting that EC cells may escape from immune surveillance by inhibiting NLRC5 and MHC-I genes expression. Furthermore, we validated that NLRC5 was expressed in both the cytoplasm and nucleus in the normal endometrium, and mainly in the latter. NLRC5 in the endometrium of EC patients was mainly expressed in the cytoplasm. Additionally, a low level of NLRC5 was correlated with positive lymph node metastasis in EC patients. The above findings prompt that NLRC5 is a target for immune escape and an elevated NLRC5 level is essential for immunotherapy in EC.

Autophagy functions as an evolutionarily conserved process to maintain cellular homeostasis. Autophagy in tumor immunity has been widely researched in recent years. However, whether autophagy promotes or prevents tumor immunity remains controversial. Studies have shown that autophagy is required for the activation of ATP-mediated dendritic cell and T cell responses by cancer cells [34]. T cells that lack autophagy restrict T cell survival and proliferation [35]. Similarly, it has been suggested that the induction of autophagy enables cells to attract antigen-presenting cells to the tumor microenvironment *via* the release of intracellular

ATP [36]. Paradoxically, some clinical trials combining chemotherapeutics with autophagy inhibitors have shown promising results in cancer patients by inducing immunogenic cell death [37]. A close relationship between autophagy and NLRs has also been reported. NLRX1 interacts with Beclin1, which is responsible for NLRX1-mediated inhibition of invasion and autophagic processes in group A streptococcus infections [38]. ATG16L1 is crucial for cytokine responses by NOD, and disruption of NOD1- or NOD2-ATG16L1 signaling causes axis-mediated pro-inflammation in Crohn's disease [39]. Many studies have reported that autophagy performs various functions in EC, such as affecting the growth of EC cells [40] and orchestrating EC therapy [41]. However, the role of autophagy in immune responses in EC is unclear. Our previous study on endometriosis revealed a negative correlation between NLRC5 and autophagy-related proteins [19]. Owing to the crucial role of autophagy in MHC-I antigen presentation [42], its potential role in NLRC5-mediated MHC-I antigen presentation pathway in EC should be considered. Our present study showed that the levels of autophagy level was upregulated in the endometrium of EC patients as compared to those in the normal endometrium. Furthermore, a high expression of LC3 was correlated with positive lymph node metastasis in EC patients. LC3 level was correlated with the FIGO stage (2009) and histological grade in EC patients. Additionally, a negative correlation was observed between LC3 and NLRC5 levels. LC3 and NLRC5 were co-localized in the cytoplasm in EC cells. CO-IP and GST pull-down assays further revealed an interaction between LC3 and NLRC5 *in vitro*. These results suggest the potential role of LC3 and NLRC5 in EC.

A loss of MHC-I has been observed in many cancers, and recent studies have indicated that a transcriptional repression of MHC-I antigen presentation to $CD8^+$ T cells in cancer can lead to immunotherapy resistance [43]. Therefore, a key approach in eliminating tumor is elevating the MHC-I antigen presentation to $CD8^+$ T cells. It has been reported that ATG proteins regulate endocytosis during antigen processing for MHC-I presentation. An absence of ATG7 and VPS34 inhibits the cross-presentation of extracellular antigens on MHC-I molecules [44]. However, a reduced MHC-I internalization in the absence of LC3 lipidation promotes intracellular antigen presentation to $CD8^+$ T cells [45]. Nevertheless, the role of LC3 in MHC-I antigen presentation pathway is still unclear. Owing to the close relationship between LC3 and NLRC5, we speculated that NLRC5 may be involved in the regulation of LC3 in MHC-I antigen presentation pathway. In this study, we validated the role of LC3 in NLRC5-mediated MHC-I antigen presentation pathway *in vitro* and *in vivo*. First, we observed that LC3 overexpression inhibited the expression levels of MHC-I genes, HLA-A, LMP2, TAP1, and β2-M at the surface of EC cells, whereas downregulation of LC3 expression promoted the expression of MHC-I genes. Furthermore, NLRC5 overexpression led to up-regulated HLA-A, LMP2, TAP1, and β2-M expressions at the surface of EC cells, and $CD8^+$ T cell proliferation in co-cultured system. Additionally, NLRC5 overexpression revealed that the negative role of LC3 in MHC-I antigen presentation pathway was restricted in HEC-1A cells and co-cultured system. Lastly, by using the xenotransplantation mice model of HEC-1A cell line, we further validated that LC3 could inhibit MHC-I antigen presentation pathway by inhibiting NLRC5 expression *in vivo*. These results suggest that LC3 inhibits the MHC-I antigen presentation pathway by directly interacting with NLRC5 in EC tissues.

Conclusion

In conclusion, our study demonstrated that LC3 level is negative correlated with NLRC5 expression in EC patients. LC3 interacted with NLRC5 to inhibit the MHC-I antigen presentation pathway, and a promotion of

NLRC5 restricted the LC3-mediated EC growth by augmenting the MHC-I antigen presentation pathway, suggesting that the strategies to reactivate exhausted antitumor immune responses by inhibiting LC3 and promoting NLRC5 may have transformational potential in the clinic in the future, at least for EC patients. These results expand the scope of the role of autophagy and NLRC5 in immune responses and identify LC3 and NLRC5 as potential targets for tumor immunotherapy in EC. Nevertheless, the sample size in the tissue microarry of our study was relatively small. In the tissue microarry of our study, we found a low level of NLRC5 and a high expression of LC3 were correlated with positive lymph node metastasis in EC patients, but Kaplan-Meier analysis showed that the expressions of LC3 and NLRC5 were not associated with cumulative survival in EC patients. Previous studies indicated that the expression of NLRC5 was correlated with survival of cancer patients [13, 46]. The inconsistent results could be because the insufficient sample size. Moreover, although we found that LC3 could directly interact with NLRC5, we were curious to understand whether LC3 could regulate NLRC5 by targeting signaling pathways. Additionally, further experiments are needed to demonstrate the effect of inhibiting LC3 and/or promoting NLRC5 expression as adjuvant therapy in the immunotherapy for EC.

Abbreviations

β2-M
Beta-2-microglobulin
CQ
Chloroquine
EC
Endometrial cancer
FIGO
International Federation of Gynecology and Obstetrics
GST
Glutathione S-transferase
HLA-A
Human leukocyte antigen A
IFN-γ
Interferon gamma
IL-2
Interleukin-2
LMP2
Low molecular mass polypeptides 2
MHC-I
Major histocompatibility complex I
NLRC5
NOD-like receptor family caspase recruitment domain containing 5
NOD
Nucleotide binding oligomerization domain
PBS

Phosphate buffered saline
qRT-PCR
Quantitative reverse transcription PCR
TAP1
Transporter associated with antigen processing 1
TBST
Tris-buffered saline with 0.1% Tween 20
TEM
Transmission electron microscopy
TNF-α
Tumor necrosis factor-alpha.

Declarations

Acknowledgements

The authors thank Editage (www.editage.com) for editing grammar, spelling, and other common errors.

Authors' contributions

Yunxia Cao and Bing Wei supervised the project. Yunxia Cao, Bing Wei, and Lei Zhan designed the overall study. Lei Zhan, Junhui Zhang, and Jing Zhang interpreted experiments. Lei Zhan and Junhui Zhang wrote the paper. Jing Zhang, Xiaojing Liu, Suding Zhu, Yuchuan Shi, and Yu He performed *in vitro* experiments and analyzed data. Jing Zhang and Xiaojing Liu performed *in vivo* experiments. Lei Zhan, Junhui Zhang, and Zhenhai Tang analyzed the data. Lei Zhan, Wenyan Wang, Yijun Fan, and Guo Chen collected and identified the endometrial specimens. All authors read and approved the final manuscript.

Funding

This work was supported by the National Nature Science Foundation of China (81802586 and 81871216), Research Fund of Anhui Institute of translational medicine (ZHYX2020A001) and Natural Science Foundation of Colleges and Universities (KJ2017A197).

Availability of data and materials

Data and materials are available upon reasonable request. Deidentified patient data are available upon reasonable request. In this case, please contact Dr. Wei (m1351565@163.com).

Declarations

Ethics approval and consent to participate

This study was approved by the Institutional Review Board of Anhui Medical University (No: 20180023). Informed consent was obtained from all the involved patients.

Consent for publication

Not applicable.

Competing interests

The authors declare that they have no competing interests.

Author details

[1]Department of Obstetrics and Gynecology, the First Affiliated Hospital of Anhui Medical University, No 218 Jixi Road, Hefei 230022, Anhui, China. [2]Department of Obstetrics and Gynecology, the Second Affiliated Hospital of Anhui Medical University, No 678 Furong Road, Hefei 230601, Anhui, China. [3]NHC Key Laboratory of Study on Abnormal Gametes and Reproductive Tract (Anhui Medical University), No 81 Meishan Road, Hefei 230032, Anhui, China. [4]Key Laboratory of Population Health Across Life Cycle (Anhui Medical University), Ministry of Education of the People's Republic of China, No 81 Meishan Road, Hefei 230032, Anhui, China. [5]Center for Scientific Research of Anhui Medical University, No 218 Jixi Road, Hefei 230022, Anhui, China.[6]Department of Gynecology, the Affiliated Maternal and Child Health Hospital of Anhui Medical University, No 15 Yimin Road, Hefei 230001, Anhui, China.

References

1. Brooks RA, Fleming GF, Lastra RR, Lee NK, Moroney JW, Son CH, et al. Current recommendations and recent progress in endometrial cancer. CA Cancer J Clin. 2019; 69(4):258–79.
2. Siegel RL, Miller KD, Jemal A. Cancer statistics, 2020. CA Cancer J Clin. 2020; 70(1):7–30.
3. Urick ME, Bell DW. Clinical actionability of molecular targets in endometrial cancer. Nat Rev Cancer. 2019; 19(9):510–21.
4. Boretto M, Maenhoudt N, Luo X, Hennes A, Boeckx B, Bui B, et al. Patient-derived organoids from endometrial disease capture clinical heterogeneity and are amenable to drug screening. Nat Cell Biol. 2019; 21(8):1041–51.
5. Arend RC, Jones BA, Martinez A, Goodfellow P. Endometrial cancer: Molecular markers and management of advanced stage disease. Gynecol Oncol. 2018; 150(3):569–80.
6. Matzner P, Sandbank E, Neeman E, Zmora O, Gottumukkala V, Ben-Eliyahu S. Harnessing cancer immunotherapy during the unexploited immediate perioperative period. Nat Rev Clin Oncol. 2020; 17(5):313–26.
7. Liu E, Marin D, Banerjee P, Macapinlac HA, Thompson P, Basar R, et al. Use of CAR-Transduced Natural Killer Cells in CD19-Positive Lymphoid Tumors. N Engl J Med. 2020; 382(6):545–53.
8. Dou Y, Kawaler EA, Cui ZD, Gritsenko MA, Huang C, Blumenberg L, et al. Proteogenomic Characterization of Endometrial Carcinoma. Cell. 2020; 180(4):729–48.

9. Makker V, Rasco D, Vogelzang NJ, Brose MS, Cohn AL, Mier J, et al. Lenvatinib plus pembrolizumab in patients with advanced endometrial cancer: an interim analysis of a multicentre, open-label, single-arm, phase 2 trial. Lancet Oncol. 2019; 20(5):711–8.
10. Theivanthiran B, Evans KS, DeVito NC, Plebanek M, Sturdivant M, Wachsmuth LP, et al. A tumor-intrinsic PD-L1/NLRP3 inflammasome signaling pathway drives resistance to anti-PD-1 immunotherapy. J Clin Invest. 2020; 130(5):2570–86.
11. Malone T, Schafer L, Simon N, Heavey S, Cuffe S, Finn S, et al. Current perspectives on targeting PIM kinases to overcome mechanisms of drug resistance and immune evasion in cancer. Pharmacol Ther. 2020; 207(107454).
12. Seliger B, Ritz U, Abele R, Bock M, Tampe R, Sutter G, et al. Immune escape of melanoma: first evidence of structural alterations in two distinct components of the MHC class I antigen processing pathway. Cancer Res. 2001; 61(24):8647–50.
13. Yoshihama S, Roszik J, Downs I, Meissner TB, Vijayan S, Chapuy B, et al. NLRC5/MHC class I transactivator is a target for immune evasion in cancer. Proc Natl Acad Sci U S A. 2016; 113(21):5999–6004.
14. Rodriguez GM, Bobbala D, Serrano D, Mayhue M, Champagne A, Saucier C, et al. NLRC5 elicits antitumor immunity by enhancing processing and presentation of tumor antigens to CD8(+) T lymphocytes. Oncoimmunology. 2016; 5(6):e1151593.
15. Puleston DJ, Simon AK. Autophagy in the immune system. Immunology. 2014; 141(1):1–8.
16. Li ZL, Zhang HL, Huang Y, Huang JH, Sun P, Zhou NN, et al. Autophagy deficiency promotes triple-negative breast cancer resistance to T cell-mediated cytotoxicity by blocking tenascin-C degradation. Nat Commun. 2020; 11(1):3806.
17. Loi M, Muller A, Steinbach K, Niven J, Barreira DSR, Paul P, et al. Macroautophagy Proteins Control MHC Class I Levels on Dendritic Cells and Shape Anti-viral CD8(+) T Cell Responses. Cell Rep. 2016; 15(5):1076–87.
18. Autophagy Inhibition Synergizes with Immunotherapy in Pancreatic Cancer. Cancer Discov. 2020; 10(6):760.
19. Zhan L, Yao S, Sun S, Su Q, Li J, Wei B. NLRC5 and autophagy combined as possible predictors in patients with endometriosis. Fertil Steril. 2018; 110(5):949–56.
20. Zhou WJ, Chang KK, Wu K, Yang HL, Mei J, Xie F, et al. Rapamycin Synergizes with Cisplatin in Antiendometrial Cancer Activation by Improving IL-27-Stimulated Cytotoxicity of NK Cells. Neoplasia. 2018; 20(1):69–79.
21. Fukuda T, Oda K, Wada-Hiraike O, Sone K, Inaba K, Ikeda Y, et al. The anti-malarial chloroquine suppresses proliferation and overcomes cisplatin resistance of endometrial cancer cells via autophagy inhibition. Gynecol Oncol. 2015; 137(3):538–45.
22. Inoue M, Ueda G, Yamasaki M, Tanaka Y, Hiramatsu K. Immunohistochemical demonstration of peptide hormones in endometrial carcinomas. Cancer-Am Cancer Soc. 1984; 54(10):2127–31.
23. Han G, Sidhu D, Duggan MA, Arseneau J, Cesari M, Clement PB, et al. Reproducibility of histological cell type in high-grade endometrial carcinoma. Mod Pathol. 2013; 26(12):1594–604.

24. Talhouk A, McConechy MK, Leung S, Yang W, Lum A, Senz J, et al. Confirmation of ProMisE: A simple, genomics-based clinical classifier for endometrial cancer. Cancer-Am Cancer Soc. 2017; 123(5):802–13.
25. Paz-Ares L, Dvorkin M, Chen Y, Reinmuth N, Hotta K, Trukhin D, et al. Durvalumab plus platinum-etoposide versus platinum-etoposide in first-line treatment of extensive-stage small-cell lung cancer (CASPIAN): a randomised, controlled, open-label, phase 3 trial. Lancet. 2019; 394(10212):1929–39.
26. Kaumaya PT, Foy KC, Garrett J, Rawale SV, Vicari D, Thurmond JM, et al. Phase I active immunotherapy with combination of two chimeric, human epidermal growth factor receptor 2, B-cell epitopes fused to a promiscuous T-cell epitope in patients with metastatic and/or recurrent solid tumors. J Clin Oncol. 2009; 27(31):5270–7.
27. Yoshida N, Ino K, Ishida Y, Kajiyama H, Yamamoto E, Shibata K, et al. Overexpression of indoleamine 2,3-dioxygenase in human endometrial carcinoma cells induces rapid tumor growth in a mouse xenograft model. Clin Cancer Res. 2008; 14(22):7251–9.
28. Mulati K, Hamanishi J, Matsumura N, Chamoto K, Mise N, Abiko K, et al. VISTA expressed in tumour cells regulates T cell function. Br J Cancer. 2019; 120(1):115–27.
29. Albacker LA, Wu J, Smith P, Warmuth M, Stephens PJ, Zhu P, et al. Loss of function JAK1 mutations occur at high frequency in cancers with microsatellite instability and are suggestive of immune evasion. Plos One. 2017; 12(11):e176181.
30. de Jong RA, Boerma A, Boezen HM, Mourits MJ, Hollema H, Nijman HW. Loss of HLA class I and mismatch repair protein expression in sporadic endometrioid endometrial carcinomas. Int J Cancer. 2012; 131(8):1828–36.
31. Perea F, Bernal M, Sanchez-Palencia A, Carretero J, Torres C, Bayarri C, et al. The absence of HLA class I expression in non-small cell lung cancer correlates with the tumor tissue structure and the pattern of T cell infiltration. Int J Cancer. 2017; 140(4):888–99.
32. Kobayashi KS, van den Elsen PJ. NLRC5: a key regulator of MHC class I-dependent immune responses. Nat Rev Immunol. 2012; 12(12):813–20.
33. Zhao MZ, Sun Y, Jiang XF, Liu L, Liu L, Sun LX. Promotion on NLRC5 upregulating MHC-I expression by IFN-gamma in MHC-I-deficient breast cancer cells. Immunol Res. 2019; 67(6):497–504.
34. Galluzzi L, Buque A, Kepp O, Zitvogel L, Kroemer G. Immunogenic cell death in cancer and infectious disease. Nat Rev Immunol. 2017; 17(2):97–111.
35. Germic N, Frangez Z, Yousefi S, Simon HU. Regulation of the innate immune system by autophagy: monocytes, macrophages, dendritic cells and antigen presentation. Cell Death Differ. 2019; 26(4):715–27.
36. Garg AD, Martin S, Golab J, Agostinis P. Danger signalling during cancer cell death: origins, plasticity and regulation. Cell Death Differ. 2014; 21(1):26–38.
37. Dummer R, Ascierto PA, Gogas HJ, Arance A, Mandala M, Liszkay G, et al. Overall survival in patients with BRAF-mutant melanoma receiving encorafenib plus binimetinib versus vemurafenib or encorafenib (COLUMBUS): a multicentre, open-label, randomised, phase 3 trial. Lancet Oncol. 2018; 19(10):1315–27.
38. Aikawa C, Nakajima S, Karimine M, Nozawa T, Minowa-Nozawa A, Toh H, et al. NLRX1 Negatively Regulates Group A Streptococcus Invasion and Autophagy Induction by Interacting With the Beclin 1-

UVRAG Complex. Front Cell Infect Microbiol. 2018; 8(403).
39. Travassos LH, Carneiro LA, Ramjeet M, Hussey S, Kim YG, Magalhaes JG, et al. Nod1 and Nod2 direct autophagy by recruiting ATG16L1 to the plasma membrane at the site of bacterial entry. Nat Immunol. 2010; 11(1):55–62.
40. Devis-Jauregui L, Eritja N, Davis ML, Matias-Guiu X, Llobet-Navas D. Autophagy in the physiological endometrium and cancer. Autophagy. 2021; 17(5):1077–95.
41. Eritja N, Chen BJ, Rodriguez-Barrueco R, Santacana M, Gatius S, Vidal A, et al. Autophagy orchestrates adaptive responses to targeted therapy in endometrial cancer. Autophagy. 2017; 13(3):608–24.
42. Munz C. Autophagy proteins in antigen processing for presentation on MHC molecules. Immunol Rev. 2016; 272(1):17–27.
43. Yamamoto K, Venida A, Yano J, Biancur DE, Kakiuchi M, Gupta S, et al. Autophagy promotes immune evasion of pancreatic cancer by degrading MHC-I. Nature. 2020; 581(7806):100–5.
44. Parekh VV, Pabbisetty SK, Wu L, Sebzda E, Martinez J, Zhang J, et al. Autophagy-related protein Vps34 controls the homeostasis and function of antigen cross-presenting CD8alpha(+) dendritic cells. Proc Natl Acad Sci U S A. 2017; 114(31):E6371-80.
45. Mintern JD, Macri C, Chin WJ, Panozza SE, Segura E, Patterson NL, et al. Differential use of autophagy by primary dendritic cells specialized in cross-presentation. Autophagy. 2015; 11(6):906–17.
46. Yoshihama S, Cho SX, Yeung J, Pan X, Lizee G, Konganti K, et al. NLRC5/CITA expression correlates with efficient response to checkpoint blockade immunotherapy. Sci Rep. 2021; 11(1):3258.

Tables

Table 1: LC3, NLRC5, HLA-A/B, LMP2, LMP7, TAP1, β2-M, and β-actin primers for qRT-PCR.

Gene	Forward	Reverse
LC3	5′-AGCAGCATCCAACCAAAATC-3′	5′- CTGTGTCCGTTCACCAACAG-3′
Beclin1	5′-AGCACCATGCAGGTGAGCTT-3′	5′-TGACACGGTCCAGGATCTTG-3′
P62	5′-CTGCTGCCTCCCTCTAATCC-3′	5′-TATTCTCCGGCTCCATCTTG-3′
NLRC5	5′-GTTCTTAGGGTTCCGTCAGCG-3′	5′- CAGTCCTTCAGAGTGGCACAGAG-3′
HLA-A	5′-TGTTCTAAAGTCCGCACGCA-3′	5′-CAGCAATGATGCCCACGATG-3′
LMP2	5′-TTGTGATGGGTTCTGATTCCCG-3′	5′-CCATGTCGGCCACGGCTTGGG-3′
TAP1	5′-TAGCTCTAGGTGTCCCGCTC-3′	5′-TCTCGGAACAAGGCAAGTCC-3′
β2-M	5′-AGCAGCATCATGGAGGTTTG-3′	5′-AGCCCTCCTAGAGCTACCTG-3′
β-actin	5′-CACCCAGCACAATGAAGATCAAGAT-3′	5′-CCAGTTTTTAAATCCTGAGTCAAGC-3′

Table 2: The guide RNA sequencing of LC3 plasmid, shRNA-LC3, NLRC5 plasmid, and shRNA-NLRC5

Gene	Forward	Reverse
LC3plasmid	5′-TGCTGCCCGACAACCACTA-3′	5′-GCTGCTTCTCACCCTTGTATCG-3′
shRNA-LC3	5′-GAGUGAGAAAGAUGAAGAU-3′	5′-AUCUUCAUCUUUCUCACUC-3′
NLRC5plasmid	5′-GGTCCTGCGTTTCTGTATGG-3′	5′-AGGCGGATGACTTGGATGCT-3′
shRNA-NLRC5	5′-AAGAACGAGAGACUCUGCCAACUGCdTdT-3′	5′-GCAGUUGGCAGAGUCUCUCGUUCUUdTdT-3′

Table 3: Demographic characteristics of leiomyoma and EC patients

Variables	No. (%) ofleiomyoma patients (n=36)	No. (%) of EC patients (n = 60)	t	p
Age, y	49.83±11.25	52.28±9.08	1.169	0.245
BMI, kg/m^2	29.56±3.02	30.46±2.45	1.601	0.113
Menopausal status				
Postmenopausal		49 (81.7)		
Premenopausal		11 (18.6)		
Histology				
Endometrioid		51 (85.0)		
Serous		9 (15.0)		
FIGO stage (2009)				
I		20 (33.3)		
II		28 (46.7)		
III		10 (16.7)		
IV		2 (3.3)		
Histological grade				
G1		36 (60.0)		
G2		18 (30.0)		
G3		6 (10.0)		
Myometrial invasion				
≤50%		50 (83.3)		
>50%		10 (16.7)		
Lymphatic node metastasis				
Positive		6 (10.0)		
Negative		54 (90.0)		

Figures

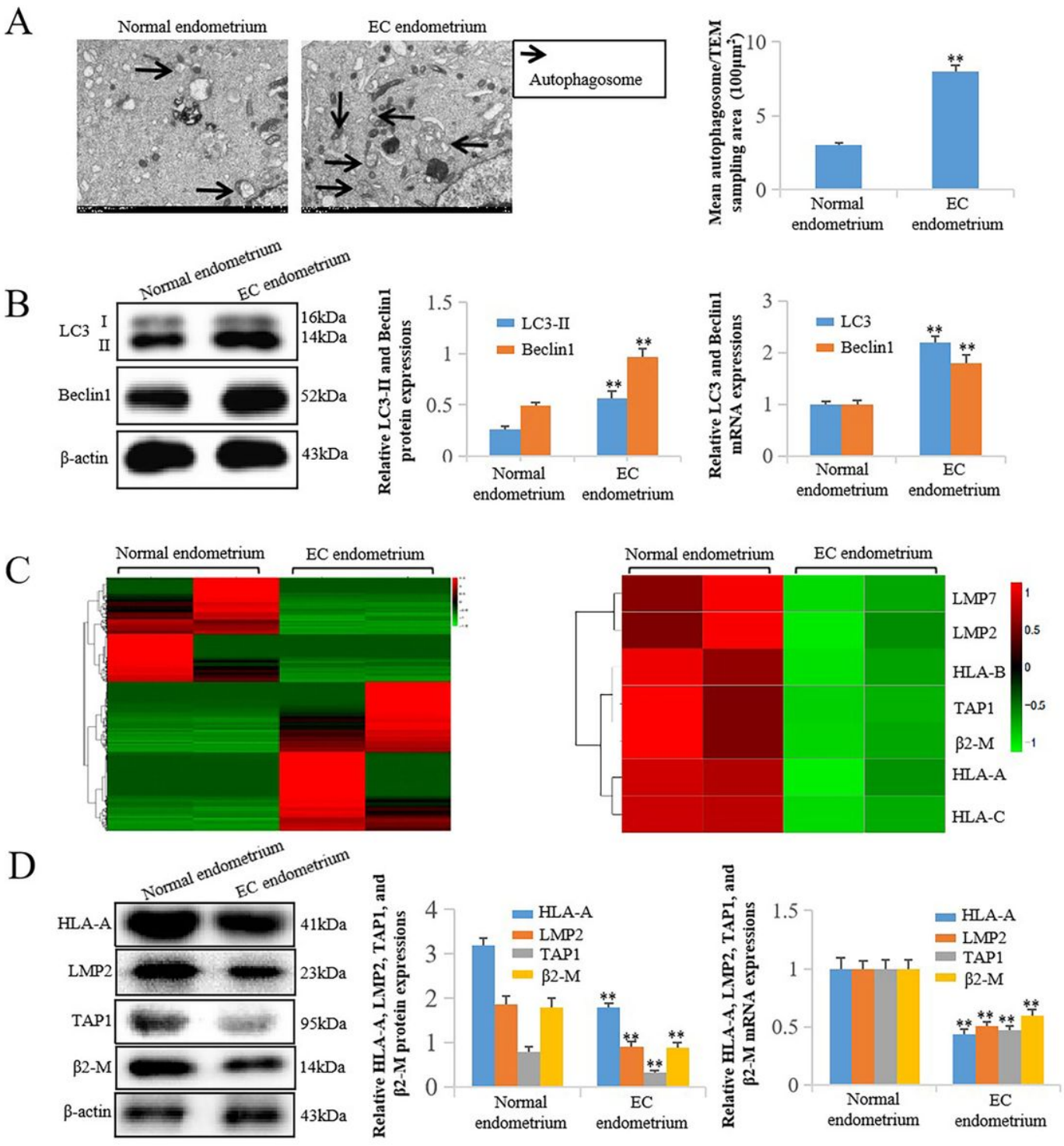

Figure 1

Autophagy is upregulated and major histocompatibility complex (MHC) I genes are inhibited in endometrial cancer (EC). A Representative transmission electron microscopy (TEM) image showing an upregulated autophagosome formation in endometrium of EC patients (n=2) as compared with normal endometrium (n=2), autophagosomes were highlighted by black arrows (scale bar: 2 μm; **P < 0.01 vs. normal endometrium). B Representative western blotting and quantitative reverse transcription PCR (qRT-PCR) results showing an upregulation of autophagy-related proteins, LC3 II and Beclin1, in endometrium of EC patients

(n=3) as compared to those in normal endometrium (n=3) (**P<0.01 vs. normal endometrium). C Representative RNA-seq sequencing showing HLA-A/B/C, LMP2/7, TAP1, β-2M were downregulated in endometrium of EC patients (n=2) as compared with those in normal endometrium (n=2). D Representative western blotting and qRT-PCR results showing an upregulation of MHC-I genes, human leukocyte antigen A (HLA-A), low molecular mass polypeptides 2 (LMP2), transporter associated with antigen processing 1 (TAP1), and beta-2-microglobulin (β2-M), in endometrium of EC patients (n=3) as compared to those in normal endometrium (n=3) (**P<0.01 vs. normal endometrium). The expression levels of mRNA were normalized according to β-actin mRNA levels, and they were calculated using the 2-ΔΔCt method. The protein expression levels were quantified using the Image J software, and they were normalized to β-actin protein levels. The results are represented as the mean ± SEM from at least three independent experiments.

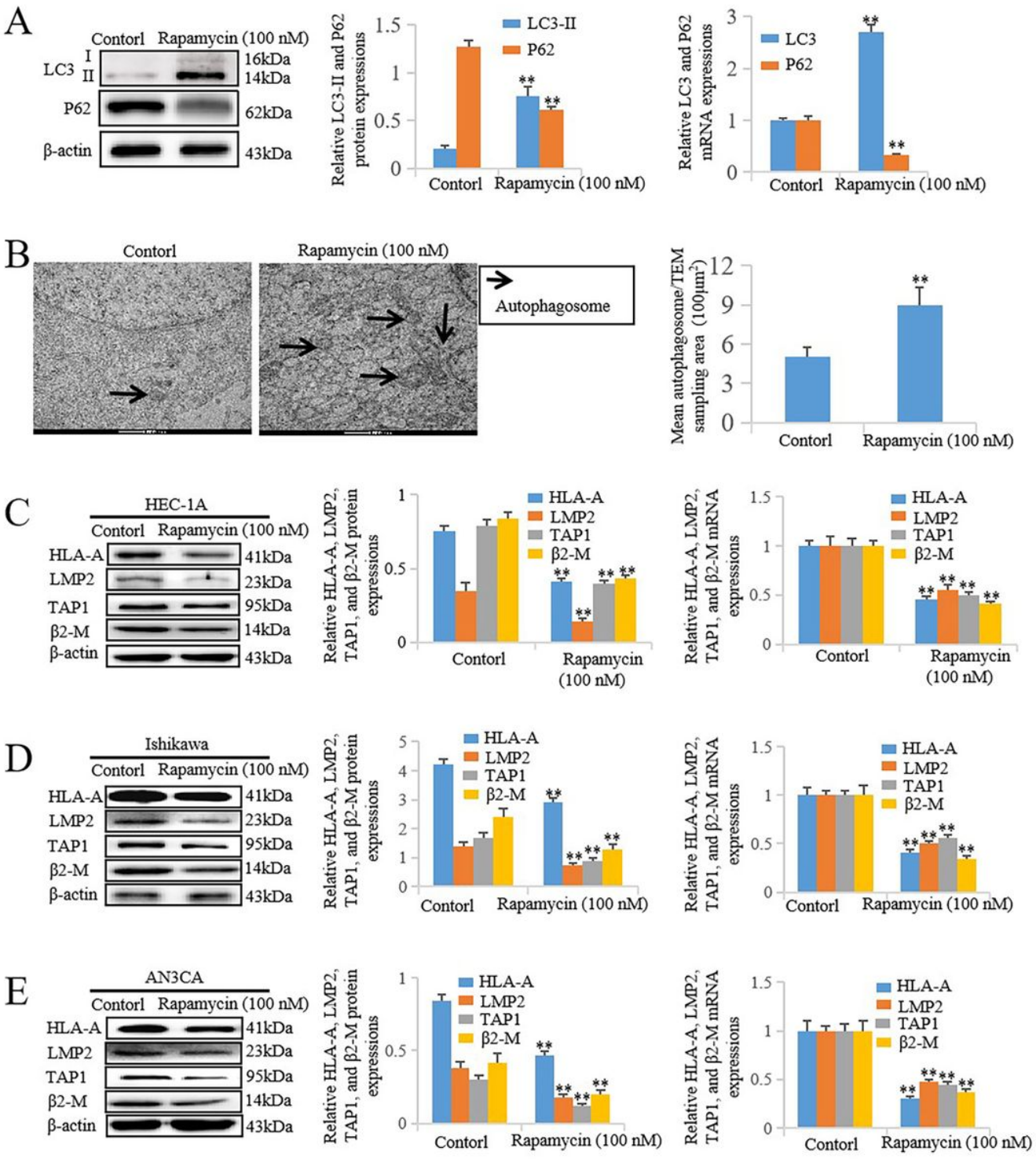

Figure 2

Promotion of autophagy by rapamycin inhibits MHC-I genes expression in EC cells. A Representative western blotting and qRT-PCR results demonstrating that a treatment with 100 nM rapamycin promotes the expression of LC3-II and inhibits the expression of P62 in HEC-1A cell (**P<0.01 vs. control group). B Representative transmission electron microscopy (TEM) showing 100 nM rapamycin significantly promotes autophagosomes formation when compared with control group, autophagosomes were highlighted by black arrows (scale bar: 2mm; **P < 0.01 vs. control group). C-E Representative western blotting and qRT-PCR

results demonstrating that a treatment with 100 nM rapamycin inhibits the expressions of HLA-A, LMP2, TAP1, and β2-M at the surface of HEC-1A, Ishikawa, and AN3CA cells (**P<0.01 vs. control group). The expression levels of mRNA were normalized with respect to β-actin mRNA levels, and they were calculated using the 2-ΔΔCt method. The protein expression levels were quantified using the Image J software, and they were normalized to β-actin protein levels. The results are represented as the mean ± SEM from at least three independent experiments.

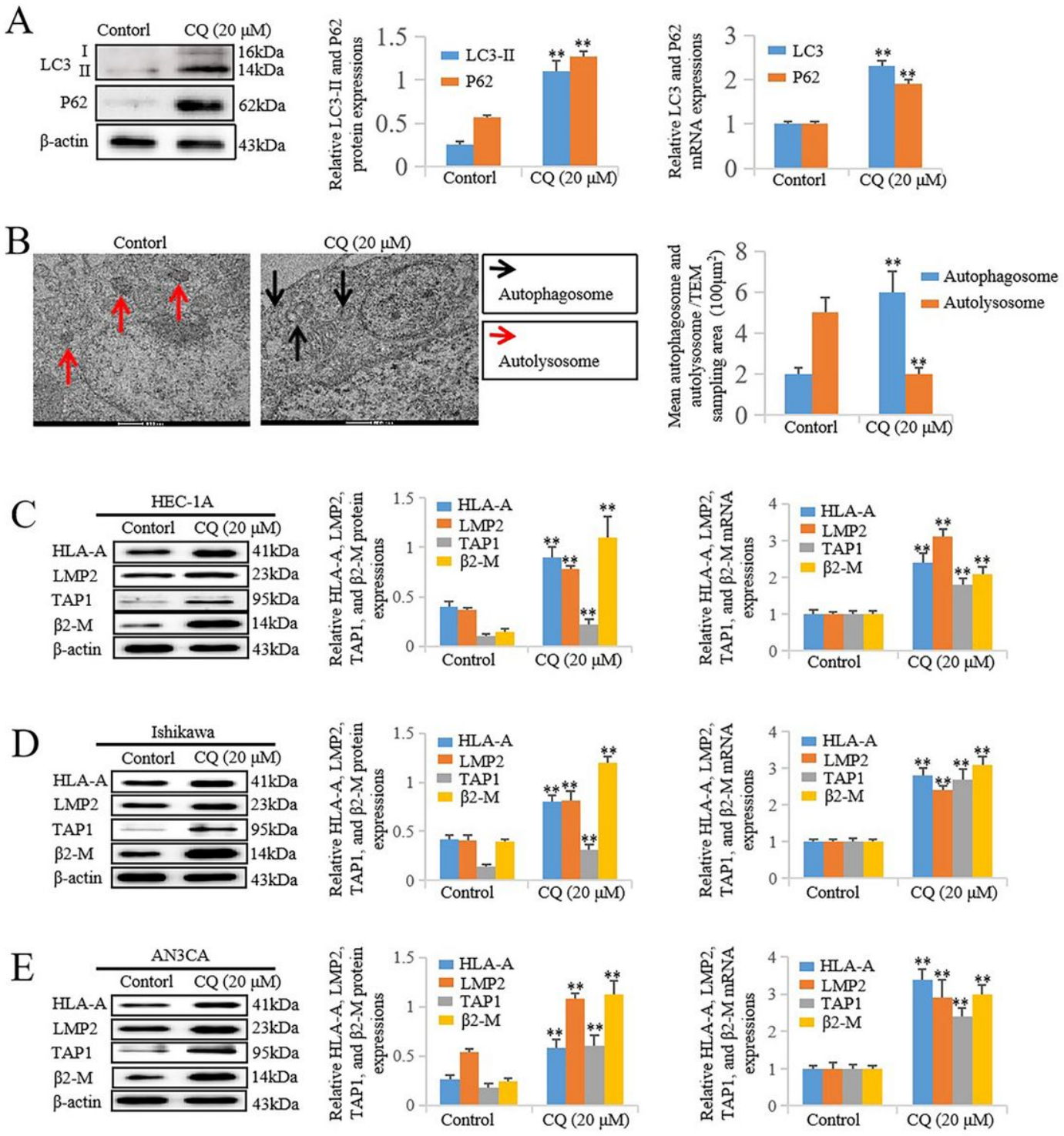

Figure 3

Inhibition of autophagy by chloroquine (CQ) promotes MHC-I genes expression in EC cells. A Representative western blotting and qRT-PCR results showing that a treatment with 20 μM CQ promotes the expressions of LC3-II and P62 in HEC-1A cell (**P<0.01 vs. control group). B Representative transmission electron microscopy (TEM) showing 20 μM CQ significantly promotes autophagosomes formation and reduces autolysosomes when compared with control group, autophagosomes were highlighted by black arrows, autolysosomes were highlighted by red arrows (scale bar: 2mm; **P < 0.01 vs. control group). C-E Representative western blotting and qRT-PCR results showing that a treatment with 20 μM CQ promotes the expressions of HLA-A, LMP2, TAP1, and β2-M at the surface HEC-1A, Ishikawa, and AN3CA cells (**P<0.01 vs. control group). The expression levels of mRNA were normalized with respect to β-actin mRNA levels, and they were calculated using the 2-ΔΔCt method. The protein expression levels were quantified using the Image J software, and they were normalized to β-actin protein levels. The results are represented as the mean ± SEM from at least three independent experiments.

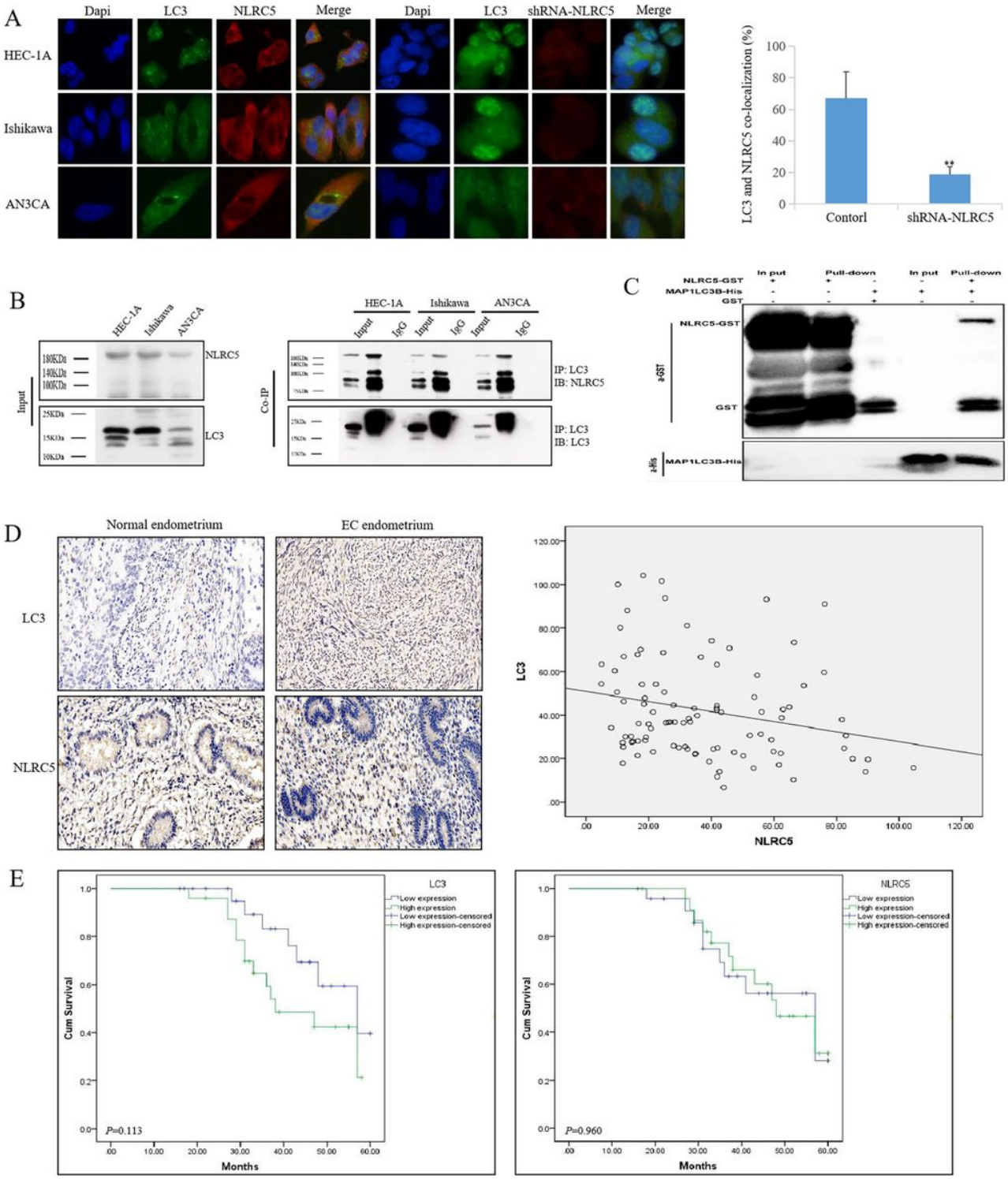

Figure 4

LC3 interacts with NLRC5. A Representative image of immunofluorescence staining showing co-localization of LC3 and NLRC5 in the cytoplasm of HEC-1A, AN3CA, and Ishikawa cells, but no co-localization of LC3 and shRNA-NLRC5 in HEC-1A, AN3CA, and Ishikawa cells (**P<0.01 vs. control group). B Co-immunoprecipitation (CO-IP) assay showed an interaction between LC3 and NLRC5 in HEC-1A, AN3CA, and Ishikawa cells. C Glutathione S-transferase (GST) pull-down assay showed an interaction between LC3 and NLRC5 in vitro. E Endometrium of normal and EC patients were subjected to immunohistochemistry analysis for LC3 and

NLRC5 levels (original magnification ×200). LC3 level was upregulated and NLRC5 was down-regulated in the endometrium of EC patients as comparison to those in the normal endometrium. Correlation analysis between LC3 and NLRC5 (r=-0.233, P<0.001). The correlation of LC3 and NLRC5 with the cumulative survival of EC patients was detected by Kaplan-Meier analysis. The results are represented as the mean ± SEM from at least three independent experiments.

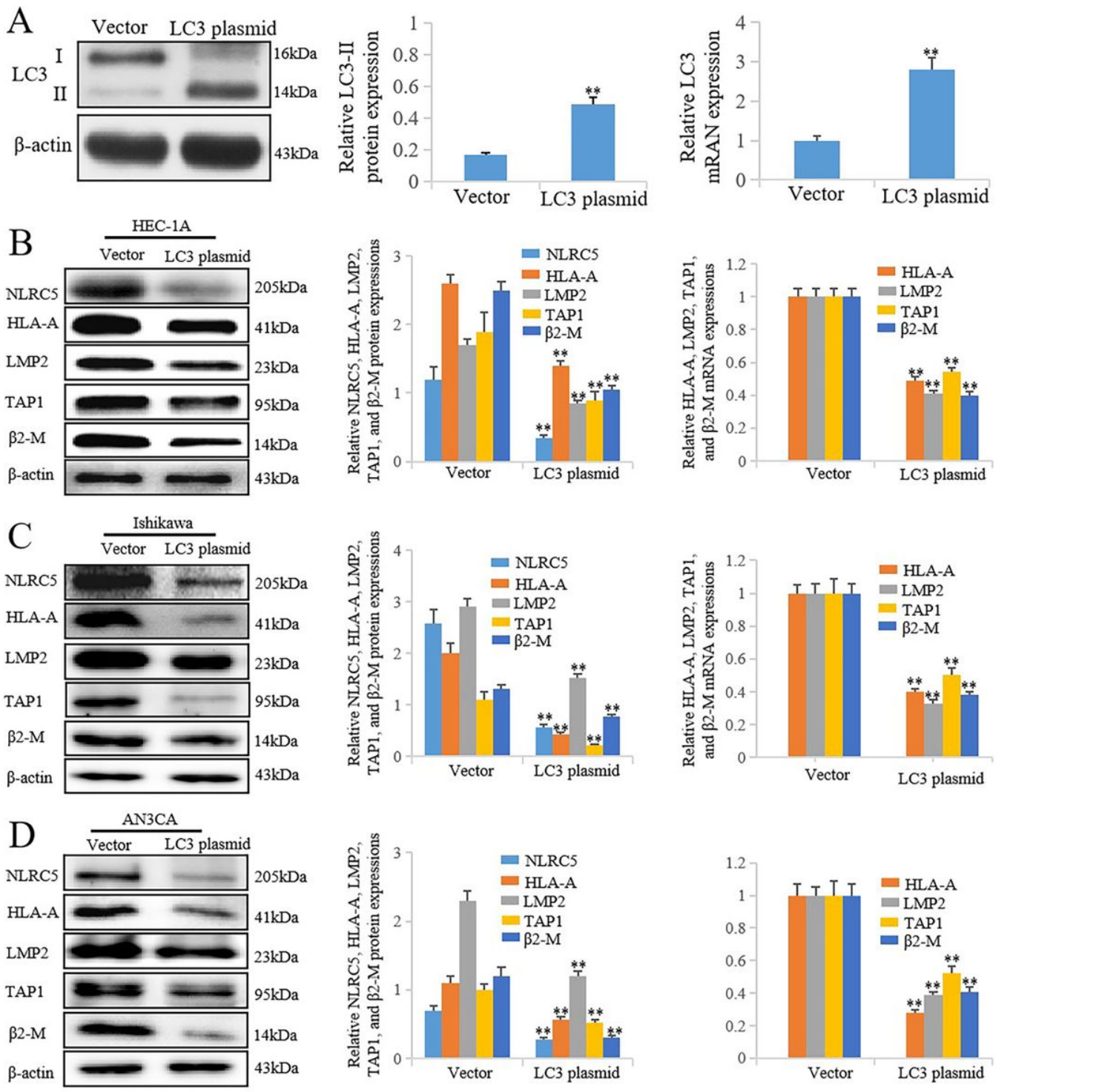

Figure 5

Overexpression of LC3 inhibits NLRC5 and MHC-I genes expressions in EC cells. A Representative western blotting, and qRT-PCR results showing successful constructions of LC3 plasmid. B-D Representative western blotting and qRT-PCR results showing overexpression of LC3 downregulates the levels of NLRC5 and MHC-I genes, HLA-A, LMP2, TAP1, and β2-M, in HEC-1A, AN3CA, and Ishikawa cells (**P<0.01 vs. vector group). The expression levels of mRNA were normalized with respect to β-actin mRNA levels, and they were calculated using the 2-ΔΔCt method. Protein expression levels were quantified using the Image J software, and they were normalized to β-actin protein levels. The results are represented as the mean ± SEM from at least three independent experiments.

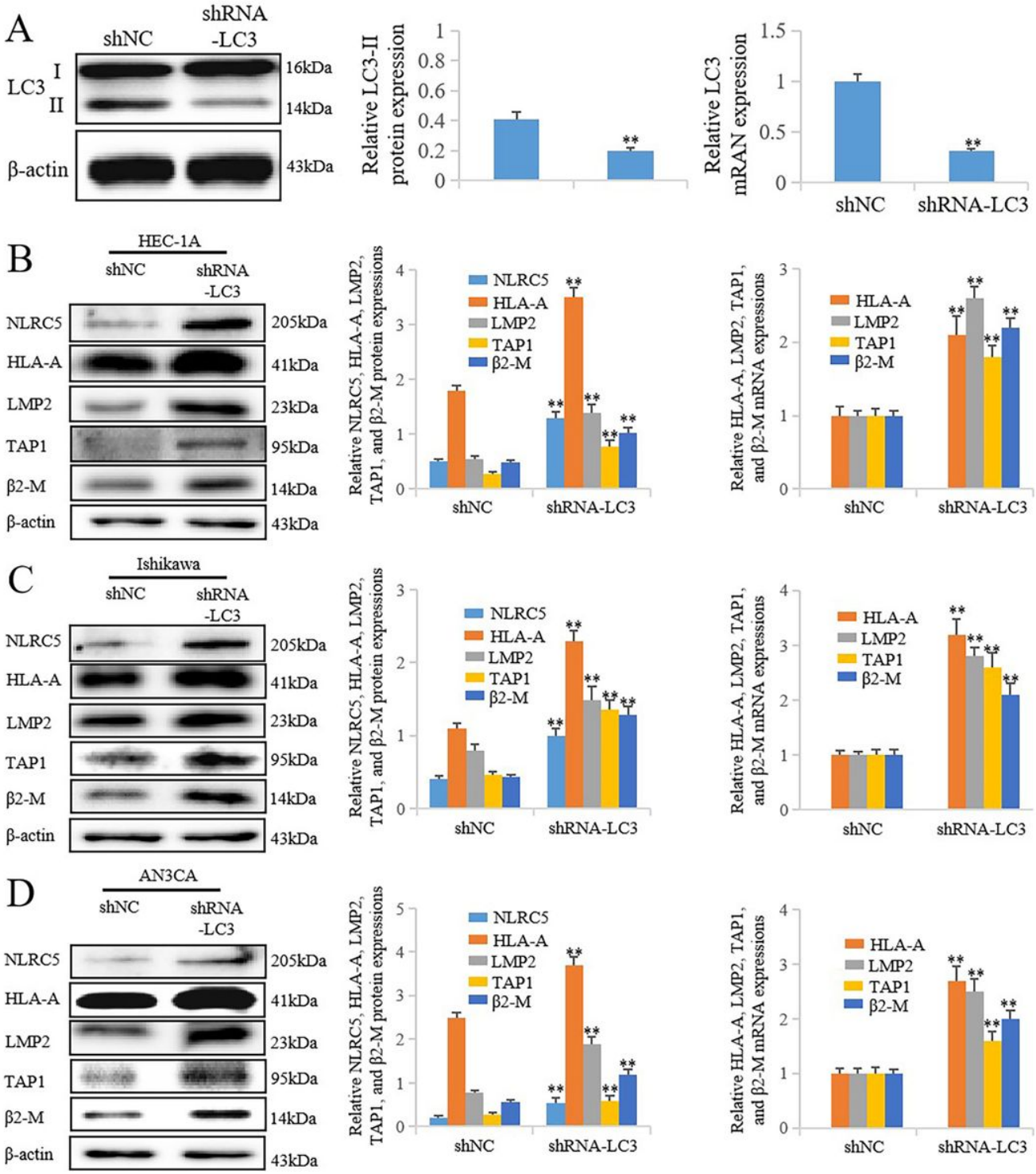

Figure 6

Inhibition of LC3 promotes NLRC5 and MHC-I genes expressions in EC cells. A Representative western blotting, and qRT-PCR results showing successful constructions of shRNA-LC3. B-D Representative western blotting and qRT-PCR results showing inhibition of LC3 upregulates the levels of NLRC5 and MHC-I genes, HLA-A, LMP2, TAP1, and β2-M, in HEC-1A, AN3CA, and Ishikawa cells (**P<0.01 vs. shNC group). The expression levels of mRNA were normalized with respect to β-actin mRNA levels, and they were calculated using the 2-ΔΔCt method. Protein expression levels were quantified using the Image J software, and they were normalized to β-actin protein levels. The results are represented as the mean ± SEM from at least three independent experiments.

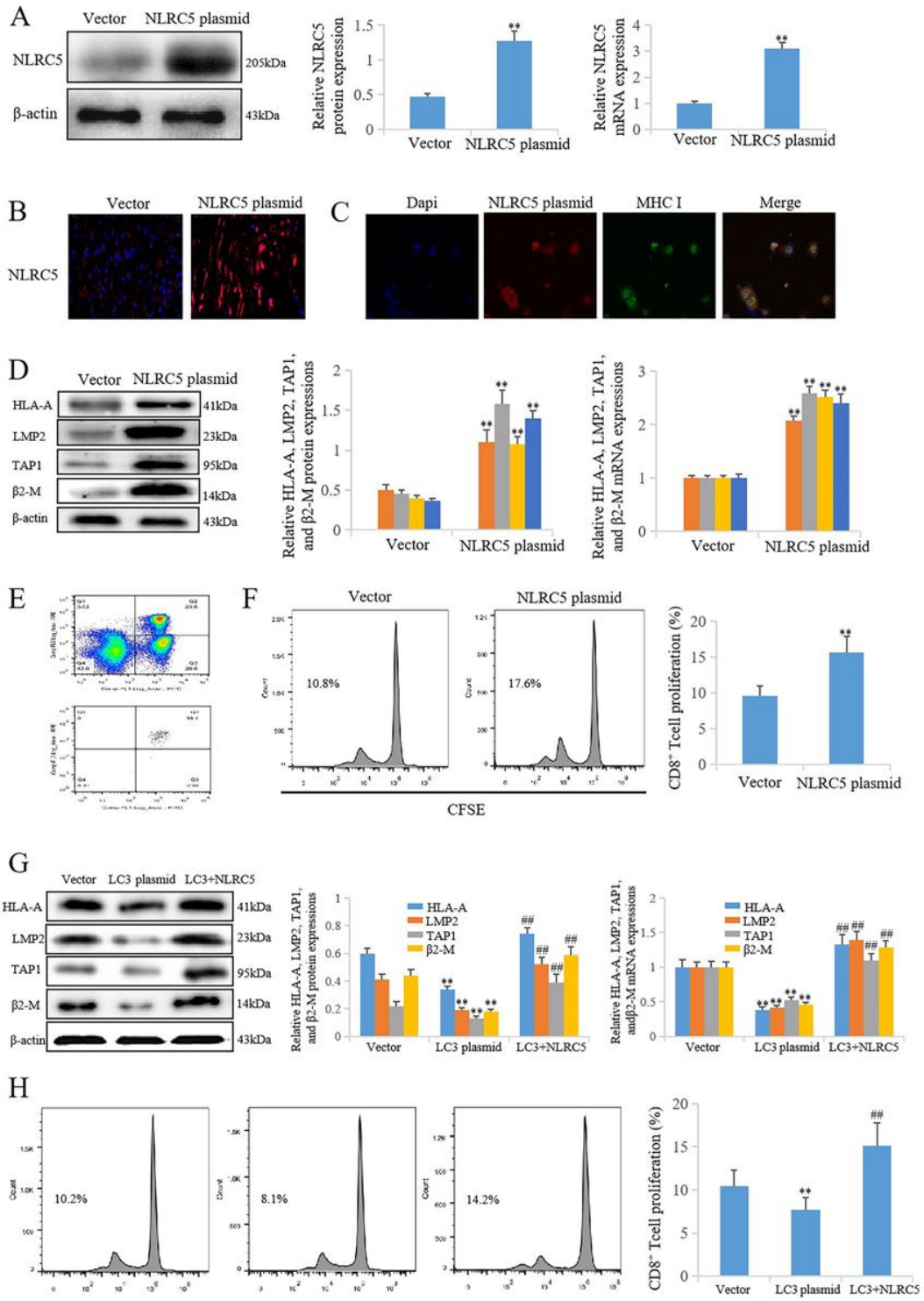

Figure 7

LC3 negative regulates MHC-I antigen presentation pathway by downregulating NLRC5 in HEC-1A cell. A Representative western blotting, and qRT-PCR results showing successful constructions of NLRC5 plasmid. B Representative image of immunofluorescence staining of NLRC5 showing NLRC5 moved to the nucleus of HEC-1A cell by NLRC5 plasmid (scale bars, 100 μm). C Representative image of immunofluorescence staining showing co-localization of NLRC5 and MHC-I in NLRC5 plasmid HEC-1A cell (scale bars, 50 μm). D Representative western blotting and qRT-PCR results showing that an upregulation of NLRC5 expression

contributes to the expressions of HLA-A, LMP2, TAP1, and β2-M, in HEC-1A cell (**P<0.01 vs. vector group). E The purity of CD8+ cell. F Representative CFSE result showing an upregulation of NLRC5 expression leads to the CD8+ T cell proliferation in HEC-1A cell and CD8+ T cell co-cultured system (**P<0.01 vs. vector group). G Representative western blotting and qRT-PCR results showing that an upregulation of NLRC5 expression restricts the negative role of LC3 in the expressions of HLA-A, LMP2, TAP1, and β2-M, in HEC-1A cell (**P<0.01 vs. vector group, ##P<0.01 vs. LC3 plasmid group). H Representative CFSE result showing the CD8+ cell proliferation was inhibited by LC3 plasmid, and upregulation of NLRC5 expression restricts the negative role of LC3 in CD8+ cell proliferation in HEC-1A cell and CD8+ T cell co-cultured system. The expression levels of mRNA were normalized with respect to β-actin mRNA levels, and they were calculated using the 2-ΔΔCt method. Protein expression levels were quantified using the Image J software, and they were normalized to β-actin protein levels. The results are represented as the mean ± SEM from at least three independent experiments.

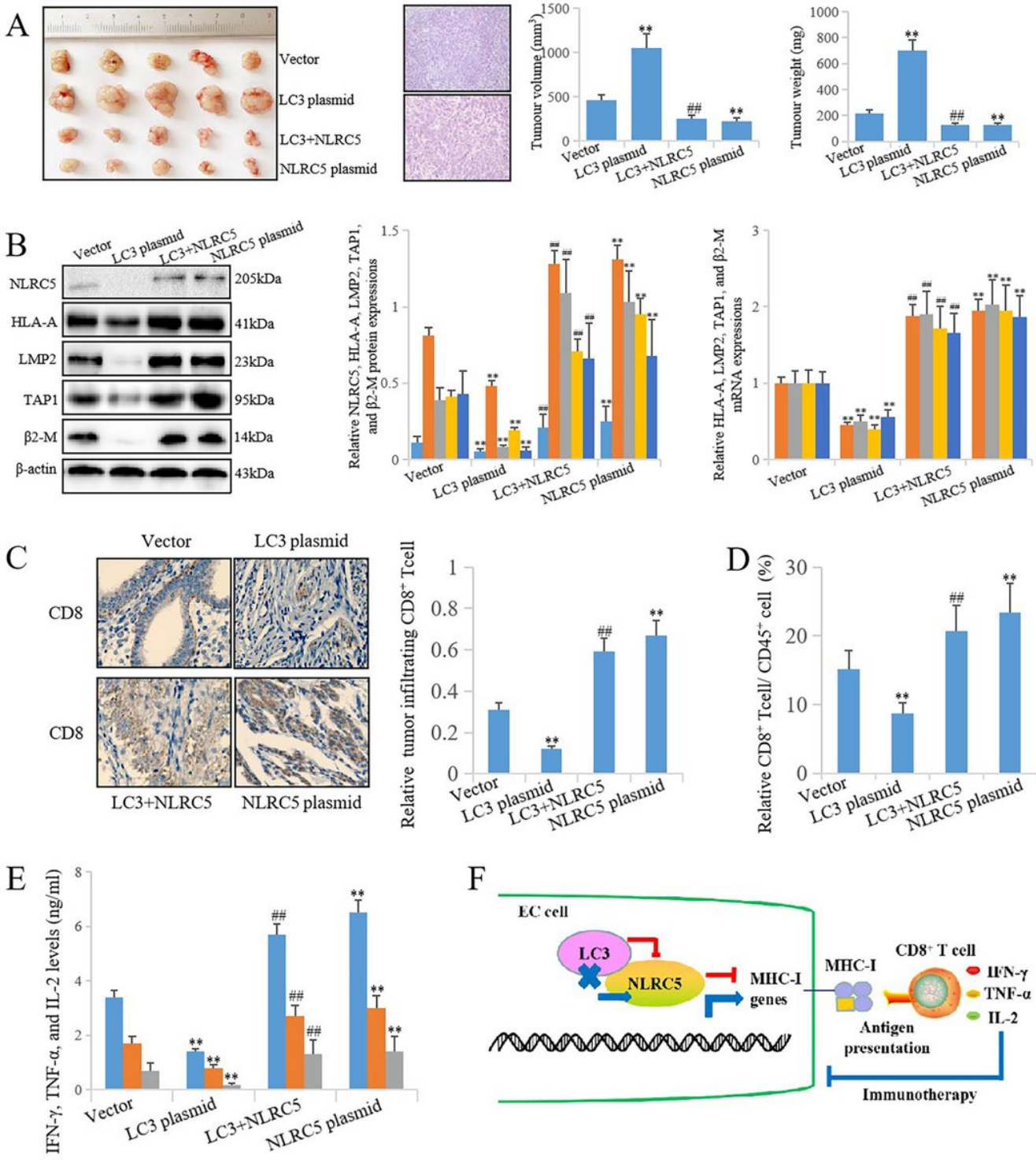

Figure 8

LC3 inhibits MHC-I antigen presentation pathway by downregulating NLRC5 in vivo. A Images of tumors; representative hematoxylin and eosin stained images of tumors (scale bars: up 200 μm and down 100 μm); volume of tumors; weight of tumors. B Representative western blotting and qRT-PCR results showing that LC3 overexpression attenuates the NLRC5 and MHC-I genes expression. NLRC5 overexpression enhances the levels of NLRC5 and MHC-I genes. An upregulation of NLRC5 expression restricts the negative role of LC3 in NLRC5 and MHC-I genes in tumors (**P<0.01 vs. vector group, ##P<0.01 vs. LC3 plasmid group). C Tumors

were subjected to immunohistochemistry analysis for CD8+ cell infiltration in tumor (original magnification ×400). LC3 overexpression attenuates CD8+ cell infiltration in tumor. NLRC5 overexpression enhances the CD8+ cell infiltration in tumor. An upregulation of NLRC5 expression restricts the negative role of LC3 in CD8+ cell infiltration in tumor (**P<0.01 vs. vector group, ##P<0.01 vs. LC3 plasmid group). D Representative flow cytometry results showing that LC3 overexpression decreases the frequency of CD8+ T cell in CD45+ cells in the peripheral blood of mice. NLRC5 overexpression augments the frequency of CD8+ T cell in CD45+ cell in the peripheral blood of mice. NLRC5 upregulation restricts the negative role of LC3 in CD8+ T cells in the peripheral blood of mice (**P<0.01 vs. vector group, ##P<0.01 vs. LC3 plasmid group). E Representative ELISA results showing that LC3 overexpression decreases the IFN-γ, TNF-α, and IL-2 levels in the peripheral blood of mice. Upregulation of NLRC5 augments the IFN-γ, TNF-α, and IL-2 levels in the peripheral blood of mice. NLRC5 overexpression restricts the negative role of LC3 in IFN-γ, TNF-α, and IL-2 production in the peripheral blood of mice (**P<0.01 vs. vector group, ##P<0.01 vs. LC3 plasmid group). F In EC, LC3 directly interacts with NLRC5 to inhibit NLRC5-mediated MHC-I antigen presentation pathway, and LC3 inhibition along with NLRC5 promotion may contribute to immunotherapy in EC by activating MHC-I antigen presentation pathway.